

CONTINUOUS TIME RANDOM WALK BASED THEORY FOR A ONE-DIMENSIONAL COARSENING MODEL

DIEGO TORREJON, MARIA EMELIANENKO AND DMITRY GOLOVATY

ABSTRACT. In this work we propose a master equation describing evolution of the velocity statistics in a one-dimensional coarsening model motivated by the studies of polycrystalline materials. The model postulates the dynamics of a large number of intervals—referred to as domains—on the real line. The length of the intervals changes during evolution and the intervals are removed from the system once their length reaches zero. The coarsening process observed in this model exhibits a number of interesting features, such as nonhomogeneous inter-arrival times between reconfiguration events and development of spatiotemporally self-similar distributions.

We generalize the standard continuous time random walk (CTRW) theory to include time-dependent jumps and subject it to time-dependent temporal rescaling to obtain an accurate non-homogeneous Poisson description of the coarsening process in the one-dimensional model. The theory leads to the evolution equation having self-similar solutions observed in simulations.

The new framework allows to accurately estimate coarsening rates and characterize resulting steady-state distribution for the domain energies described by a power law of a uniformly distributed quantity. Although derived here in the context of a one-dimensional systems, this work naturally extends to higher dimensional CTRW coarsening models.

1. INTRODUCTION

Coarsening models are used to describe dynamics of physical systems consisting of multiple domains, where some regions grow at the expense of others. The average size of domains grows over time, hence the network experiences “coarsening”. While this process is very complex in three dimensions, lower-dimensional models often offer advantages in elucidating certain features of dynamics and are extremely instrumental at the early stages of theory development. Smoluchowski’s coagulation [1], Mullins model [2, 3] and curvature-driven model by Lazar et al [4, 5] are only some of the one-dimensional examples that can be found in literature. Here we focus our attention on a one-dimensional model originally introduced in [6], which is different from those in [1]-[5] in that it is aimed at capturing topological changes in the evolving grain boundary network compared to the curvature-driven effects. This choice is motivated by the widely accepted fact that topological reconfigurations play a critical role during texture development in polycrystals.

Scaling theories characterize scaling laws of self-similar behavior of statistical distributions harvested from simulations or experiments. The procedure normally amounts to postulating

2010 *Mathematics Subject Classification.* Primary: 82B41; Secondary: 82D35.

Key words and phrases. CTRW, coarsening, polycrystals, self-similarity, master equation.

Received 29/10/2016, accepted 01/11/2016.

DT was supported by the National Science Foundation Graduate Research Fellowship under Grant No. DGE-1356109. ME was partially supported by National Science Foundation grant DMS-1056821.

suitable scaling hypothesis (ansatz) and deriving corresponding scaling exponents describing the self-similar form for the quantities of interest. Our goal is to carry out this task in the context of a one-dimensional model, which we do by means of interrogating the large-scale coarsening simulation for a variety of initial conditions and parameter choices. Having evidence of self-similar behavior, we invoke the probabilistic description of the velocity jump process first introduced in [6], which allows us to recover the scaling exponents. What emerges as a result of this work is a coherent theory in a form of a generalized master equation capturing self-similar features of the system evolution.

An attempt to develop such theory in the context of materials applications dates back to Mullins [7, 8] and has been a focus of many recent investigations [9]-[15]. Relatively speaking, starting from a discrete model, the continuous time random walk (CTRW) approach presented herein attempts to avoid any physical assumptions and is grounded in purely statistical and probabilistic analysis of numerical observations.

CTRW theory has found applications in many areas of science and technology. In particular, it is widely used in financial applications such as in insurance risk theory, in Gibrat's model for growth and inequality, and in pricing financial markets [16]-[19]. In biology, it is applied to derive aggregation models [20, 21]. In physics, CTRWs are useful in modeling transport in fusion plasmas [22], in reaction-diffusion models [23]-[25], and in processes involving anomalous diffusion [26]-[31].

In the standard CTRW formalism, a random walker inter-arrival times and jump sizes are drawn from a certain transition probability density [18, 20, 27]. In [23, 25], Angstman et al. derive a generalized CTRW master equation on a lattice with non-stationary jump sizes and space dependent inter-arrival times for a single particle and for an ensemble of particles undergoing reactions whilst being subject to an external force field. In [32], a CTRW master equation on a lattice is derived for the delayed forcing and instantaneous forcing under a biased nearest-neighbor jumps assumption. In [22], Milligen et al derive a generalized CTRW master equation with space- and time dependence on the jump sizes and space dependence on the inter-arrival times.

Our derivation of the generalized master equation happens to fall under the typical scenario in which the transition probability is separable [20, 23, 27, 33], but we are faced with the challenge of having non-homogeneous inter-arrival times and time-dependent jump sizes. We use appropriate time-dependent scalings to deal with both of these complications. While the exact form of these laws differs from one system to another, the overall framework remains the same as long as one can accurately compute the jump sizes and inter-arrival times statistics from a given simulation.

The paper is organized as follows. In Section 2 we generalize the standard CTRW theory to the case of time-dependent jump sizes and derive the corresponding master equation. In Section 3 we show that our coarsening model falls precisely under the class of CTRW processes treated in Section 2. This allows us to derive the exact expressions for the self-similar solutions in Section 4. We implement the resulting steady state equation numerically and show agreement with simulation.

1.1. Simulation description. In this section we define and analyze the properties of a simple coarsening network - a system of domains represented by intervals on the circle, as introduced in [6] and analyzed in a series of works [34, 35]. Following the same set-up, we assume that each domain is described by its length and a scalar "energy density" parameter. Only nearest neighbor interactions between the domains are considered, with the strength of the interactions dependent on the energy densities of the neighboring domains.

To fix ideas, for a given $L > 0$ consider a circle of circumference L or, equivalently, an interval $[0, L] \subset \mathbb{R}$ with periodic boundary conditions. Randomly select n points $\{x_i\}_{i=1}^n \subset [0, L]$ with $x_i \leq x_{i+1}$ for $i = 1, \dots, n-1$ and the point x_{n+1} identified with the point x_1 . Given the periodicity assumption, the interval $[0, L]$ is thus subdivided into n sub-intervals $[x_i, x_{i+1}]$, $i = 1, \dots, n$ of lengths $l_i = x_{i+1} - x_i$, $i = 1, \dots, n-1$ and $l_n = L + x_1 - x_n$, respectively. Note that the locations and the number of points will vary during evolution, however the total length L of all intervals remains fixed. Further, if a partition point leaves $[0, L]$ through $x = 0$, it immediately re-enters $[0, L]$ at $x = L$ and vice versa.

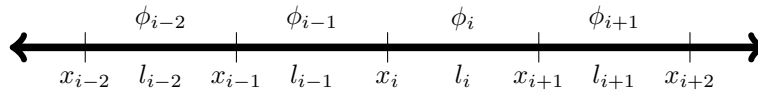


FIGURE 1. Set-up of the one dimensional coarsening model where $\{x_i\}_{i=1}^n$, $\{l_i\}_{i=1}^n$, $\{\phi_i\}_{i=1}^n$ denote domain boundaries, domain lengths, and energy densities, respectively.

For each interval $[x_i, x_{i+1}]$, $i = 1, \dots, n$, we select a random number $\phi_i \in \mathbb{R}$ as seen in Figure 1. Here the interval $[x_i, x_{i+1}]$ for $i = 1, \dots, n$ can be thought of as a “domain” and the points x_i, x_{i+1} as the domain boundaries (DBs).

We define the total energy of the one-dimensional system by

$$(1.1) \quad E(t) = \sum_{i=1}^n \phi_i [x_{i+1}(t) - x_i(t)]$$

and consider the gradient flow dynamics given by the system of ordinary differential equations

$$(1.2) \quad \dot{x}_i = \phi_i - \phi_{i-1}, \quad i = 2, \dots, n, \quad \text{and} \quad \dot{x}_1 = \phi_1 - \phi_n.$$

In what follows, we consider a non-negative energy density of the form

$$(1.3) \quad \phi_i = \phi(\alpha_i) = |\alpha_i|^\gamma, \quad \gamma > 0.$$

Here the parameter α_i , initially chosen for each domain according to the uniform random distribution in the interval $(-\pi/4, \pi/4)$, does not change during the lifetime of the corresponding domain.

The rate of change of the domain length—referred to as a velocity of a domain $i = 1, \dots, n$ —can be computed from the relation

$$(1.4) \quad v_i = \dot{x}_{i+1} - \dot{x}_i = \phi(\alpha_{i+1}) + \phi(\alpha_{i-1}) - 2\phi(\alpha_i).$$

The set of domain velocities changes only at the times of collisions between adjacent DBs eliminating the domains between these boundaries; we call each event of this type a *disappearance event*. The velocity corresponding to the collapsed domain is then removed from the list of domain velocities while the velocities of its neighbors are adjusted appropriately. Note that the lengths of the individual domains vary linearly in time between the disappearance events and depend entirely on the respective domain velocities.

An important feature of the thermodynamics of coarsening in materials is that it is energy dissipative. The reduced gradient flow model (1.2) is specifically designed to enforce dissipation, as verified in [6].

1.2. Stabilization of statistics. In this section we describe the results of numerical simulations of a system containing a large number of domains. The simulations reveal the set of coarse-grained characteristics of the system that develop over time which we will use in subsequent sections to establish an appropriate statistical model.

First, we find that there is a transient relaxation stage that occurs early in the simulation, when energetically unfavorable domains are quickly eliminated from the system. After the relaxation stage, we observe stabilization of the respective statistics of relative domain lengths, DB velocities, domain velocities, and energy densities. The duration of the relaxation stage varies depending on the value of γ . As γ decreases, as seen in Figure 2, we observe that the steady-state distribution of the relative energy density is farther from the initial distribution. Hence, it takes longer for the distribution to stabilize for lower values of γ . Note that the initial distribution of the energy density, in Figure 2, has a jump due to the fact that α is chosen in the interval $(-\pi/4, \pi/4)$.

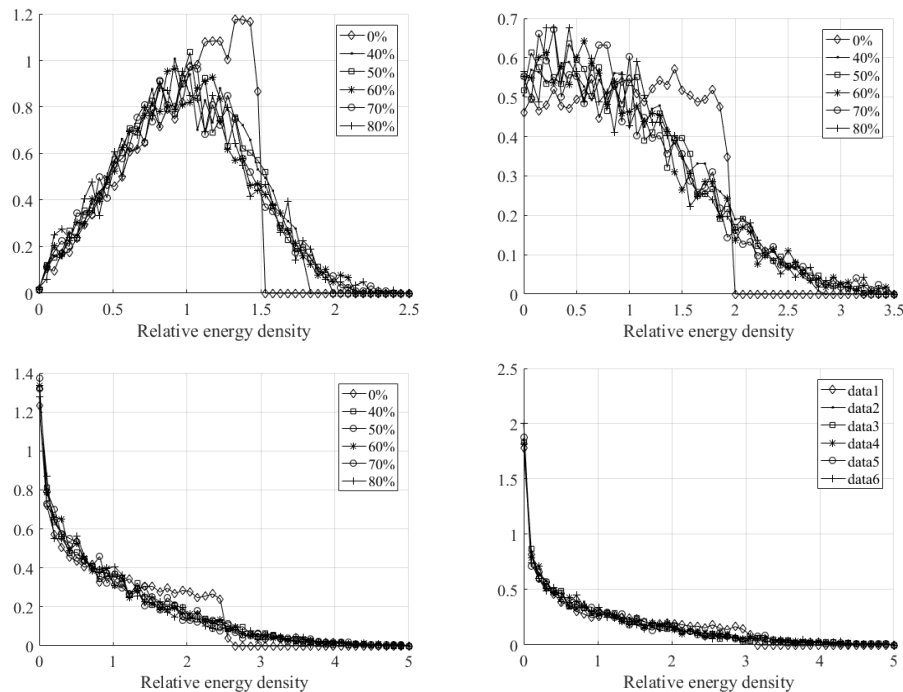


FIGURE 2. Relative energy density distribution at various stages of evolution as indicated by the percentage of domains eliminated from the system. Top left: $\gamma = 0.5$. Top right: $\gamma = 1$. Bottom left: $\gamma = 1.5$. Bottom right: $\gamma = 2$.

Following the analysis done in [6], we reproduce the inter-arrival times and jump sizes statistics, as seen in Figure 3. While the inter-arrival times plots are clearly of exponential type with growing means (cf. [6]), the distributions of jump sizes behave in a less intuitive manner, prompting a further investigation.

The feature of primary interest in the present study is the development of the self-similar regime in this coarsening model, as alluded to in the introduction. Indeed, with a suitable

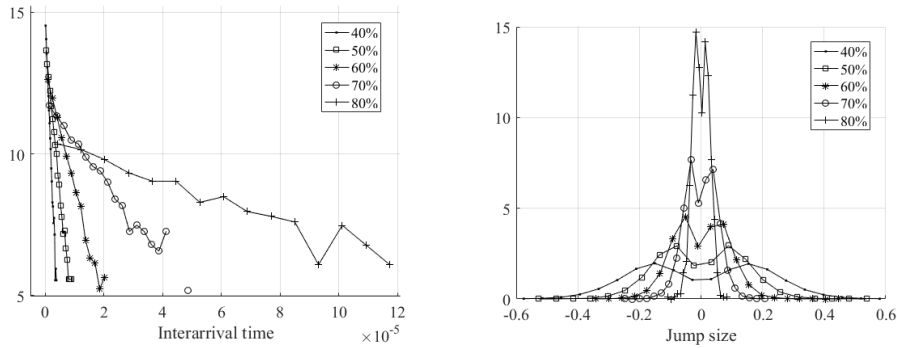


FIGURE 3. Inter-arrival times and jump sizes for $\gamma = 2$ at various stages of evolution as indicated by the percentage of domains eliminated from the system. Left: Semi-log plot of inter-arrival times. Right: Evolution of jump sizes.

choice of spatiotemporal scaling laws resulting distributions of velocities and energies exhibit self-similarity. We give numerical evidence of this fact in Section 4, in Figures 9 and 10. Based on the stochastic properties of the appropriate random variables that we deduce from numerical experiments, we develop a modification of the continuous time random walk (CTRW) theory. This theory leads to an integral-differential equation that accurately models the evolution of the one-dimensional system of domains in the self-similar regime. Above all, it gives a formal characterization for the stochastic processes driving coarsening dynamics, as we are about to describe in the sections that follow.

2. GENERALIZATION OF CTRW THEORY

2.1. Homogeneous master equation. The concept of CTRW theory became popular half a century ago as a rather general microscopic model for diffusion processes. Unlike discrete time random walks, in the CTRW the number of jumps made by a walker during a time interval is a stochastic—often a homogeneous Poisson—process. The continuous time random walk was first introduced by Montroll and Weiss [36], Montroll and Scher [37], and later on by Klafter and Silbey [38].

In the standard CTRW setting, both the inter-arrival times and the jump sizes are assumed to be independent and identically distributed. Another typical assumption is that the jump size are statistically independent of the inter-arrival times; the corresponding process is referred to as a decoupled CTRW.

We begin this section with a generalization of the CTRW framework obtained by dropping the assumption of identically distributed jump sizes. The CTRW model is based on the idea that the jump size and inter-arrival time are drawn from a joint p.d.f. $\tilde{\theta}$ which will be referred to as the transition probability density function. Hence the transition probability of taking a jump from velocity v_0 at time τ_0 to velocity v at time τ is represented by $\tilde{\theta}(v - v_0, \tau - \tau_0, \tau)$. We assume that the transition p.d.f. is *separable*

$$(2.1) \quad \tilde{\theta}(v - v_0, \tau - \tau_0, \tau) = \tilde{\mu}(v - v_0, \tau) \tilde{w}(\tau - \tau_0) = \tilde{\mu}(\Delta v, \tau) \tilde{w}(s),$$

with $s = \tau - \tau_0$ and $\Delta v = v - v_0$. Here

$$\int_{\mathbb{R}} \tilde{\mu}(\Delta v, \tau) d(\Delta v) = 1 \text{ for all } \tau > 0 \text{ and } \int_0^{\infty} \tilde{w}(s) ds = 1.$$

We also introduce the function

$$\tilde{\psi}(\tau) = 1 - \int_0^{\tau} \tilde{w}(s) ds$$

that evaluates the probability that a walker remains at a given position at least for the time period τ .

Let $\tilde{p}(v, \tau)$ be the probability density function such that $\tilde{p}(v, \tau) dv$ gives the probability that the position of a walker lies inside the interval $(v, v + dv)$ at time τ . We have the following lemma.

Lemma 1. *The probability distribution function $\tilde{p}(\cdot, \tau)$ satisfies the master equation*

$$(2.2) \quad \tilde{p}(v, \tau) = \tilde{\psi}(\tau)F(v) + \int_0^{\tau} \int_{\mathbb{R}} \tilde{w}(\tau - \tau') \tilde{\mu}(\Delta v, \tau') \tilde{p}(v - \Delta v, \tau') d(\Delta v) d\tau'$$

for all $v \in \mathbb{R}$ and $\tau > 0$, where $F(\cdot)$ is the initial configuration of walkers.

Proof. We first state an evolution equation for the occupancy density function $P(v, \tau|0)$ defined so that $P(v, \tau|0)dv$ is the probability that the position of a walker (who was at the origin at time $\tau = 0$) lies in the interval $(v, v + dv)$ at time τ . The occupancy density $P(v, \tau|0)$ satisfies the following renewal equation

$$(2.3) \quad P(v, \tau|0) = \tilde{\psi}(\tau)\delta(v) + \int_0^{\tau} \int_{\mathbb{R}} \tilde{w}(\tau - \tau') \tilde{\mu}(\Delta v, \tau') P(v - \Delta v, \tau'|0) d(\Delta v) d\tau'.$$

Intuitively, the first term accounts for the walker who fails to move from the starting position at $v = 0$ at least until time τ . The integral expresses the fact that a walker found at the position v at time τ arrived to v after making his last jump from $v - \Delta v$ where he was at time τ' . If instead the walker starts at $v_0 \neq 0$, i.e., $P(v, 0|v_0) = \delta(v - v_0)$, then (2.3) changes to

$$(2.4) \quad P(v, \tau|v_0) = \tilde{\psi}(\tau)\delta(v - v_0) + \int_0^{\tau} \int_{\mathbb{R}} \tilde{w}(\tau - \tau') \tilde{\mu}(\Delta v, \tau') P(v - \Delta v, \tau'|v_0) d(\Delta v) d\tau'.$$

If the initial state of the walker is given by an initial probability density distribution $\tilde{p}(v, 0) = F(v)$, then

$$\tilde{p}(v, \tau) = \int_{\mathbb{R}} P(v, \tau|v_0) F(v_0) dv_0.$$

Hence $\tilde{p}(v, \tau)$ satisfies the master equation

$$\tilde{p}(v, \tau) = \tilde{\psi}(\tau)F(v) + \int_0^{\tau} \int_{\mathbb{R}} \tilde{w}(\tau - \tau') \tilde{\mu}(\Delta v, \tau') \tilde{p}(v - \Delta v, \tau') d(\Delta v) d\tau',$$

as follows from (2.4). □

Lemma 2. *Let the waiting times in Lemma 1 be exponentially distributed according to $\tilde{w}(\tau) = \tilde{\lambda}e^{-\tilde{\lambda}\tau}$. Then*

$$(2.5) \quad \frac{\partial}{\partial \tau} \tilde{p}(v, \tau) = \tilde{\lambda} \int_{\mathbb{R}} \tilde{\mu}(\Delta v, \tau) [\tilde{p}(v - \Delta v, \tau) - \tilde{p}(v, \tau)] d(\Delta v).$$

Proof. It is convenient to work with equation (2.2) in Laplace space with respect to time. We denote the Laplace variable as u and the Laplace transform of any function $\tilde{f}(\tau)$ by $\hat{f}(u)$. Taking the Laplace transform of (2.2),

$$\begin{aligned} \mathcal{L}_\tau[\tilde{p}(v, \tau)](u) &= \mathcal{L}_\tau[\tilde{\psi}(\tau)F(v)](u) + \mathcal{L}_\tau \left[\int_{\mathbb{R}} \int_0^\tau \tilde{w}(\tau - \tau') \tilde{\mu}(\Delta v, \tau') \tilde{p}(v - \Delta v, \tau') d\tau' d(\Delta v) \right] (u) \\ (2.6) \quad &= F(v) \frac{1 - \hat{w}(u)}{u} + \hat{w}(u) \mathcal{L}_\tau \left[\int_{\mathbb{R}} \tilde{\mu}(\Delta v, \tau) \tilde{p}(v - \Delta v, \tau) d(\Delta v) \right] (u). \end{aligned}$$

After some algebra manipulation of (2.6),

$$(2.7) \quad \hat{\Phi}(u)(u\hat{p}(v, u) - F(v)) + \hat{p}(v, u) = \mathcal{L}_\tau \left[\int_{\mathbb{R}} \tilde{\mu}(\Delta v, \tau) \tilde{p}(v - \Delta v, \tau) d(\Delta v) \right] (u)$$

where

$$\hat{\Phi}(u) = \frac{1 - \hat{w}(u)}{u\hat{w}(u)}.$$

Taking the inverse Laplace transform of (2.7),

$$(2.8) \quad \int_0^\infty \Phi(\tau - \tau') \frac{\partial}{\partial \tau} \tilde{p}(v, \tau') d\tau' + \tilde{p}(v, \tau) = \int_{\mathbb{R}} \tilde{\mu}(\Delta v, \tau) \tilde{p}(v - \Delta v, \tau) d(\Delta v).$$

$\Phi(\tau)$ denotes the memory function of the continuous time random walk [17]. Equation (2.8) reduces to a differential equation if the process is Markovian, i.e., the waiting time is exponentially distributed with rate function $\tilde{\lambda}$. Then

$$\tilde{w}(\tau) = \tilde{\lambda} e^{-\tilde{\lambda}\tau} \Rightarrow \hat{w}(u) = \frac{\tilde{\lambda}}{u + \tilde{\lambda}} \Rightarrow \hat{\Phi}(u) = \frac{1}{\tilde{\lambda}} \Rightarrow \Phi(\tau) = \frac{1}{\tilde{\lambda}} \delta(\tau).$$

Under these assumptions, (2.8) derives

$$\frac{\partial}{\partial \tau} \tilde{p}(v, \tau) = \tilde{\lambda} \int_{\mathbb{R}} \tilde{\mu}(\Delta v, \tau) [\tilde{p}(v - \Delta v, \tau) - \tilde{p}(v, \tau)] d(\Delta v).$$

□

Remark 1. Denote \tilde{n}_t as the counting process of jumps by a walker. Assuming exponentially and identically distributed inter-arrival times implies that \tilde{n}_t is a homogeneous Poisson process with the arrival rate $\tilde{\lambda}$.

Remark 2. Equation (2.5) can also be obtained by differentiating (2.2) and simplifying the resulting expression.

2.2. Nonhomogeneous master equation. The following theorem based on [39] relates the homogeneous Poisson process with the nonhomogeneous Poisson process,

Theorem 1. *If $\{\tilde{n}_\tau, \tau \geq 0\}$ is a homogeneous Poisson process with rate $\tilde{\lambda} = 1$, then $\{n_t = \tilde{n}_{m(t)}, t \geq 0$ with $m(t) = \int_0^t \lambda(s) ds\}$ is a nonhomogeneous Poisson process with rate $\lambda(t)$.*

As a simple consequence of Theorem 1 and Lemma 2, we get the following analog of (2.5).

Corollary 1. *The probability distribution function $p(\cdot, t) = \tilde{p}(\cdot, m(t))$ satisfies the master equation*

$$(2.9) \quad \frac{\partial}{\partial t} p(v, t) = \lambda(t) \int_{\mathbb{R}} [p(v - \Delta v, t) - p(v, t)] \mu(\Delta v, t) d(\Delta v),$$

for all $v \in \mathbb{R}$ and $t > 0$ with $\mu(\Delta v, t) = \tilde{\mu}(\Delta v, m(t))$, and $\lambda(t)$ being the arrival rate of the nonhomogeneous Poisson process n_t .

Proof. Denote by \tilde{n}_τ the homogeneous Poisson process with arrival rate $\tilde{\lambda}$. Without loss of generality assume $\tilde{\lambda} = 1$; otherwise include $\tilde{\lambda}$ as a factor in $\lambda(t)$. We apply Theorem 1 with $\tau = m(t)$ where $m(t) = \int_0^t \lambda(s) ds$. Then $n_t = \tilde{n}_{\tau(t)}$ is a nonhomogeneous Poisson process with rate $\lambda(t)$. We have that (2.5) holds with the rate $\tilde{\lambda} = 1$, that is

$$\frac{\partial}{\partial \tau} \tilde{p}(v, \tau) = \int_{\mathbb{R}} [\tilde{p}(v - \Delta v, \tau) - \tilde{p}(v, \tau)] \tilde{\mu}(\Delta v, \tau) d(\Delta v).$$

In terms of the time variable t this equation takes the form (2.9). □

3. COARSENING MODEL AS A CTRW

3.1. Ensemble statistics vs. individual statistics. In this section, we apply the theory developed in Section 2 to our one-dimensional coarsening model. Considering each DB velocity as a walker, we can denote by n_t the stochastic process counting the number of jumps experienced by this walker up to time t . The rate associated with this process will be denoted by $\lambda(t)$. Let \mathcal{M}_t be the stochastic process describing the evolution of velocity jump sizes with probability density function $\mu(\Delta v, t)$ and \mathcal{V}_t be the stochastic process describing the evolution of velocities with probability density function $p(v, t)$. Here v and Δv denote DB velocity and DB velocity jump size, respectively. In what follows, we demonstrate the stochastic processes \mathcal{M}_t , \mathcal{V}_t , and n_t satisfy the assumptions that lead to (2.9). Hence, we expect p , μ , and λ to be connected via (2.9).

Experimentally, we observe a collection of domains at any given time, so any statistics that we collect is the statistics for the entire collection. In order to recover the quantities for a single walker, we therefore need to relate the statistical properties of a collection to the statistical properties of an individual walker. Numerical experiments given in [6] indicate that the coarsening model dynamics is ergodic and the DB velocities are i.i.d. at any given time. We conclude that the DB velocity distribution in the system of many boundaries is described by the same equation (2.9) as that for a single boundary.

In order to recover the arrival rate for a walker corresponding to velocity jumps of a single DB, consider the stochastic process N_t counting the number of domains at time t . Then, as it is shown in Theorem 3 in the Appendix, the arrival rate $\lambda_N(t)$ is related to the arrival rate of a single walker by

$$\lambda_N(t) = 2N(t)\lambda(t),$$

where $N(t)$ is the number of domains at time t and the factor of 2 comes from the fact that each disappearance event corresponds to two DB velocity jumps.

3.2. Separability. We validate the assumption that the joint distribution of non-homogeneous inter-arrival times and velocity jump sizes is separable, i.e., $\theta(\Delta v, s, t) = w(s, t)\mu(\Delta v, t)$ for any $t > 0$. We start by checking the correlation of jump sizes and the inter-arrival times at different stages of the coarsening simulation. In Figure 4, we plot the p -values and the correlation coefficients corresponding to the test of no correlation between jump sizes and interarrival times. Since the majority of p -values are greater than 0.05 and the correlation coefficients are small, there is no evidence of correlation in the data.

In order to conclusively show independence between the jump sizes and the inter-arrival times, in Figure 5, we provide a scatter plot for two-dimensional data at the different stages

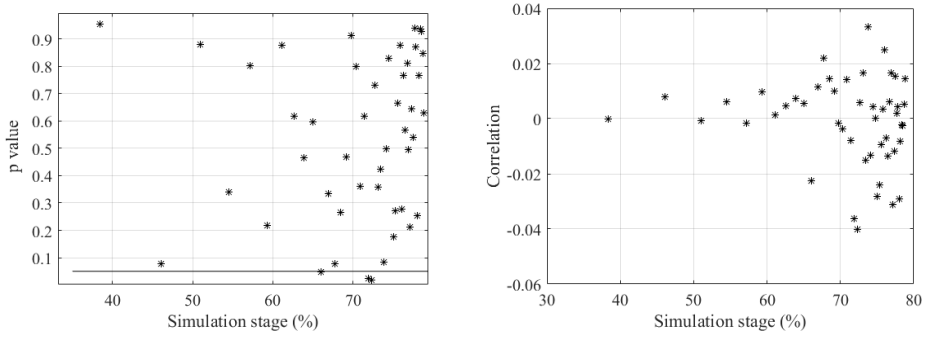


FIGURE 4. Left: p-values for the null hypothesis of no correlation between jump sizes and inter-arrival times at different stages of the simulation for $\gamma = 2$. p-values below black line denote significant values. Right: Correlation coefficients between jump sizes and inter-arrival times at different stages of the simulation.

of simulation. In addition, in Figure 6, we show that the joint distribution of jump sizes and inter-arrival times is essentially equal to the product of the corresponding marginals. Although not presented here, the separability hypothesis was also validated for other values of γ .

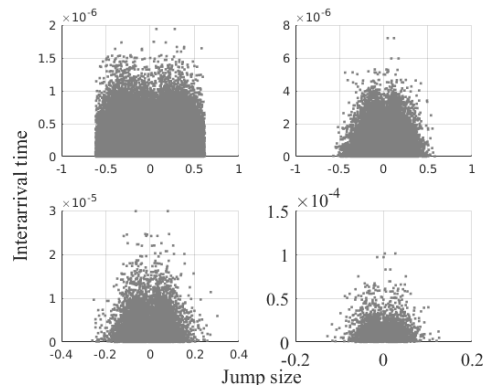


FIGURE 5. A scatter plot of the inter-arrival times against jump sizes at 20%(top left), 40%(top right), 60%(bottom left), and 80%(bottom right) of the simulation for $\gamma = 2$.

3.3. Nonhomogeneous Poisson process validation. First we show that the counting process N_t constitutes a nonhomogeneous Poisson process. According to Definition 2, N_t is a nonhomogeneous Poisson process if the following two conditions hold:

- (a) given a countable, disjoint collection $\{I_j\}$ of measurable subsets of \mathbb{R}^+ , then $\{N_{I_j}\}$ is a collection of independent random variables.

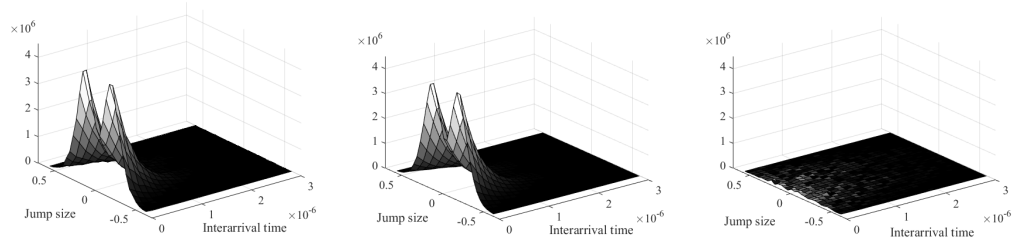


FIGURE 6. Left: Joint distribution of the jump sizes and inter-arrival times. Middle: Product of the jump size marginal and the inter-arrival time marginal. Right: Absolute error between the joint distribution and the product of marginals. All the statistics were computed at 40% of the simulation for $\gamma = 2$.

- (b) if $I \subset \mathbb{R}^+$ is measurable, then N_I has a Poisson distribution with arrival rate $\int_I \lambda_N(s) ds$.

In order to test that N_t (or, equivalently, $N_0 - N_t$) is a nonhomogeneous Poisson process, we partition the time interval of the simulation into sub-intervals $\{I_j\}$. As evident from Figure 7, the distribution of $N_0 - N_t$ on $\{I_j\}$ resembles the Poisson distribution. The independence condition is validated in Figure 8. Although not presented here, both hypotheses were also validated for other values of γ .

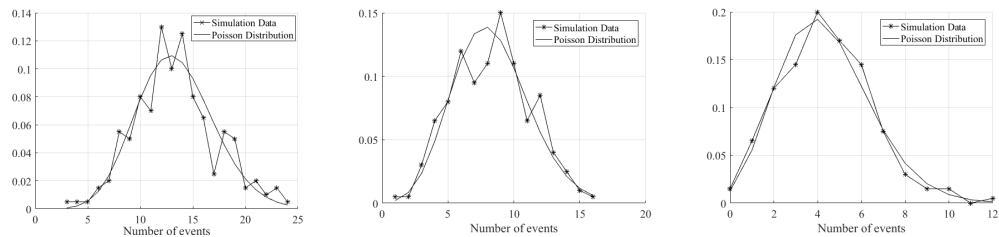


FIGURE 7. Comparing the distribution of $N_0 - N_{I_j}$ with the Poisson distribution for $\gamma = 2$. Left: At 30% of the simulation. Middle: At 50% of the simulation. Right: At 80% of the simulation.

4. SELF-SIMILARITY OF SOLUTIONS

4.1. Scaling laws. In this section, we show that following the relaxation stage, the processes \mathcal{M}_t and \mathcal{V}_t become self-similar.

Definition 1. Let the process S_t be a stochastic process with probability density function $s(x, t)$. Suppose there exists $t^* \geq 0$, representing the end of the relaxation stage, such that

$$\forall t \geq t^* \exists b > 0 : \{S_t\} \stackrel{d}{=} \{bS_{t^*}\} \Leftrightarrow \forall t \geq t^* \exists b > 0 : s(x, t) = \frac{1}{b} s\left(\frac{x}{b}, t^*\right).$$

Then we say that S_t is self-similar.

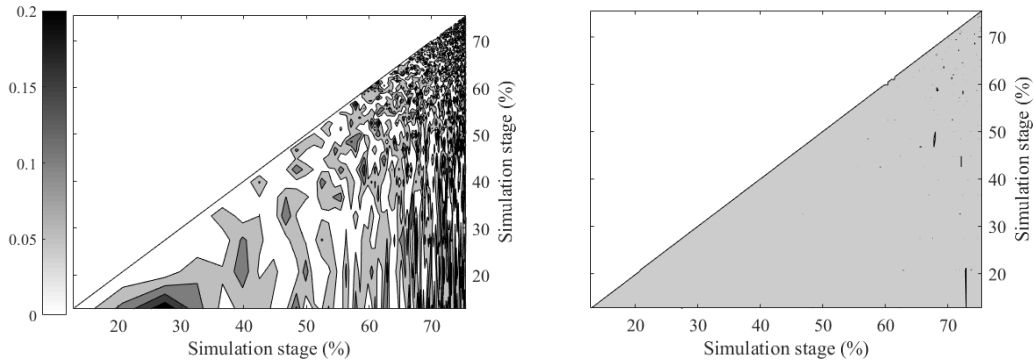


FIGURE 8. Validating the independence condition for $N_0 - N_t$ for $\gamma = 2$. Left: Correlation values between $N_0 - N_{I_i}$ and $N_0 - N_{I_j}$ for i and j at different stages of the simulation. The colorbar denotes the magnitude of the correlation. Right: p -values for the null hypothesis of no correlation between $N_0 - N_{I_i}$ and $N_0 - N_{I_j}$ for i and j at different stages of the simulation. In the gray area, there is no statistical evidence of correlation.

As seen in Figures 9 and 10, processes \mathcal{V}_t and \mathcal{M}_t indeed become self-similar, i.e.,

$$(4.1) \quad p(v, t) = b(t)p(b(t)v, t^*) = b(t)p_0(b(t)v), \quad \forall t \geq t^*$$

and

$$(4.2) \quad \mu(\Delta v, t) = b(t)\mu(b(t)\Delta v, t^*) = b(t)\mu_0(b(t)v), \quad \forall t \geq t^*$$

after the relaxation stage corresponding to $t < t^*$. Here $b : (t^*, \infty) \rightarrow \mathbb{R}^+$ is a time-dependent coefficient of self-similarity the explicit form of which will be established next.

4.2. Steady state equation. Now we are in a position to justify self-similar behavior of the one-dimensional coarsening model (1.2). As shown in Section 3, the dynamics of N_t is governed by equation (2.9). Further, we have the following theorem.

Theorem 2. *Equation (2.9) admits a self-similar solution (p_0, μ_0) if the jump size and the velocity processes $\mathcal{M}_t, \mathcal{V}_t$, respectively, are self-similar. The scaling parameter $b(t)$ satisfies*

$$(4.3) \quad \begin{cases} b'(t) = -\beta\lambda(t)b(t), & t \geq t^* \\ b(t^*) = 1, \end{cases}$$

where β is a parameter independent of t but possibly dependent on γ . Moreover, the self-similar solution pair (p_0, μ_0) satisfies

$$(4.4) \quad \beta[xp_0(x)]' = - \int_{-\infty}^{\infty} \mu_0(y)[p_0(x-y) - p_0(x)]dy.$$

Proof. Since \mathcal{M}_t and \mathcal{V}_t are self-similar processes, then $p(v, t)$ and $\mu(\Delta v, t)$ have self-similar forms as shown in (4.1) and (4.2) with scaling parameter $b(t)$. Plugging (4.1) and (4.2) in

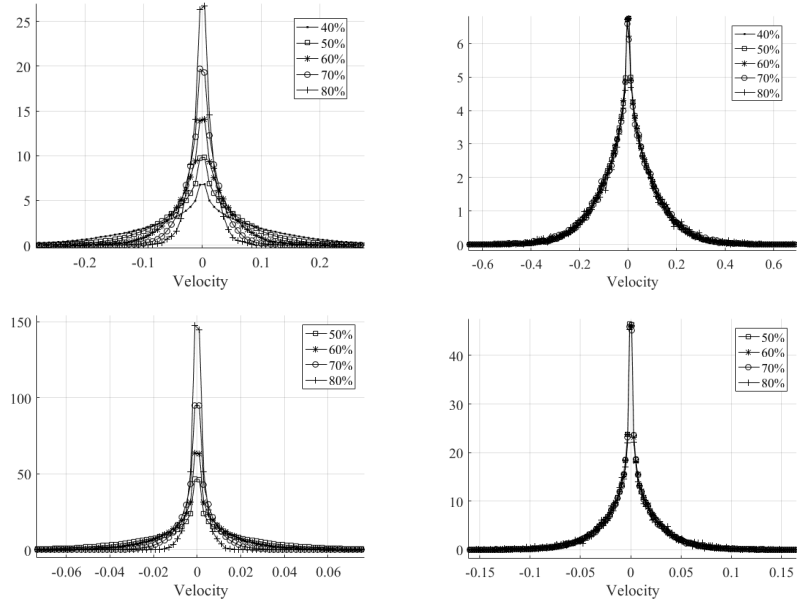


FIGURE 9. Velocity distribution at different stages of the simulation. Left column: Unscaled. Right column: Scaled to reveal self-similarity. The scaling parameter is $b(t) = \left(\frac{E(N_t)}{E(N_{t^*})}\right)^\gamma$. Top row: $\gamma = 2$. Bottom row: $\gamma = 3$.

(2.9),

$$(4.5) \quad b(t)p'_0(b(t)v)b'(t)v + b'(t)p_0(b(t)v) \\ = \lambda(t) \int_{-\infty}^{\infty} b(t)\mu_0(b(t)\Delta v)b(t) [p_0(b(t)(v - \Delta v)) - p_0(b(t)v)] d(\Delta v).$$

Letting $x = b(t)v$ and $y = b(t)\Delta v$ and simplifying using (4.3),

$$\begin{aligned} -\beta x p'_0(x)b(t)\lambda(t) - \beta b(t)\lambda(t)p_0(x) &= b(t)\lambda(t) \int_{-\infty}^{\infty} \mu_0(y)[p_0(x - y) - p_0(x)]dy \\ -\beta x p'_0(x) - \beta p_0(x) &= \int_{-\infty}^{\infty} \mu_0(y)[p_0(x - y) - p_0(x)]dy \\ \beta[xp_0(x)]' &= - \int_{-\infty}^{\infty} \mu_0(y)[p_0(x - y) - p_0(x)]dy. \end{aligned}$$

□

Remark 3. If p_0 and μ_0 satisfy the integro-differential equation (4.4), then (4.1) and (4.2) solve (2.9).

Corollary 2. We can represent $b(t)$ as follows

$$(4.6) \quad b(t) = \left(\frac{E(N_t)}{E(N_{t^*})}\right)^{\frac{\beta}{2}}.$$

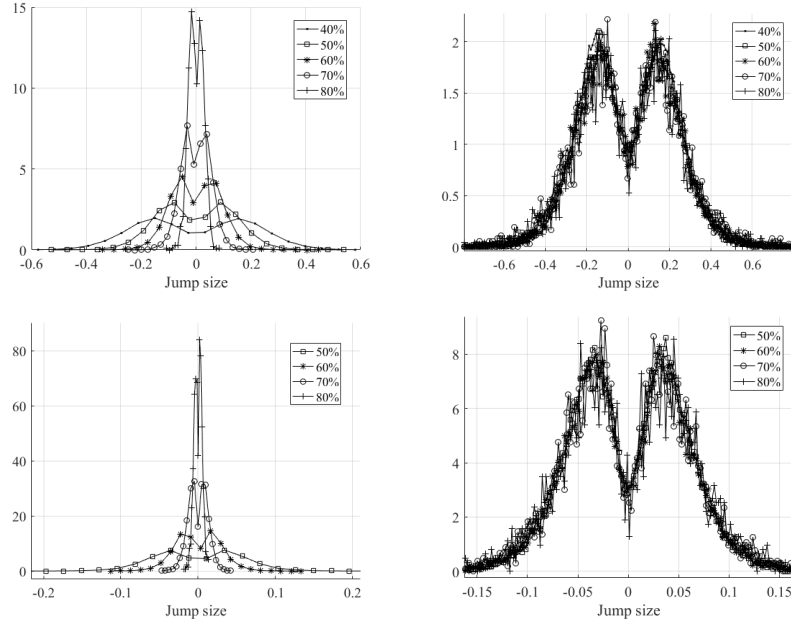


FIGURE 10. Velocity jump size distribution at different stages of the simulation. Left column: Unscaled. Right column: Scaled to reveal self-similarity. The scaling parameter is $b(t) = \left(\frac{\mathbb{E}(N_t)}{\mathbb{E}(N_{t^*})} \right)^\gamma$. Top row: $\gamma = 2$. Bottom row: $\gamma = 3$.

Proof. According to (4.3),

$$b(t) = \exp \left(-\beta \int_0^t \lambda(s) ds \right).$$

Then

$$\begin{aligned} b(t) &= \exp \left(-\beta \int_0^t \lambda(s) ds \right) \\ &= \exp \left(-\frac{\beta}{2} \int_0^t \frac{\lambda_N(s)}{\mathbb{E}(N_s)} ds \right) \\ &= \exp \left(-\frac{\beta}{2} \int_0^t -\frac{d}{ds} \mathbb{E}(N_s) \frac{1}{\mathbb{E}(N_s)} ds \right) \\ &= \exp \left(-\frac{\beta}{2} \log \left(\frac{\mathbb{E}(N_{t^*})}{\mathbb{E}(N_t)} \right) \right) \\ &= \left(\frac{\mathbb{E}(N_t)}{\mathbb{E}(N_{t^*})} \right)^{\frac{\beta}{2}}. \end{aligned}$$

□

4.3. Comparison with simulations. We find it convenient to write (4.4) in the form,

$$(4.7) \quad \beta x p_0(x) = \int_0^x p_0(u) du - \int_{-\infty}^{\infty} \mu_0(y) \left(\int_0^{x-y} p_0(u) du \right) dy \\ + \int_{-\infty}^{\infty} \mu_0(y) \left(\int_0^{-y} p_0(u) du \right) dy.$$

We can show that the third integral on the right hand side of equation (4.7) vanishes because both p_0 and μ_0 are even functions, as observed in Figures 9 and 10, i.e.,

$$(4.8) \quad \int_{-\infty}^{\infty} \mu_0(y) \left(\int_0^{-y} p_0(u) du \right) dy \\ = \int_0^{\infty} \mu_0(y) \left(\int_0^{-|y|} p_0(u) du \right) dy + \int_{-\infty}^0 \mu_0(y) \left(\int_0^{|y|} p_0(u) du \right) dy \\ = - \int_0^{\infty} \mu_0(y) \left(\int_{-|y|}^0 p_0(u) du \right) dy + \int_{-\infty}^0 \mu_0(y) \left(\int_0^{|y|} p_0(u) du \right) dy = 0.$$

Hence, we can simplify (4.7),

$$(4.9) \quad \beta x p_0(x) = \int_0^x p_0(u) du - \int_{-\infty}^{\infty} \mu_0(y) \left(\int_0^{x-y} p_0(u) du \right) dy.$$

In Figure 11, we show that p_0 and μ_0 derived from our simulation satisfy (4.9) with the choice of $\beta = \frac{\gamma}{2}$ for $\gamma = 2$ and $\gamma = 3$, where the integrals are computed using the trapezoidal rule. The two graphs in each figure correspond to the left hand side (LHS) and right hand side (RHS) of the equation (4.9), respectively. It must be noted that when testing other values of γ , we observe a very good agreement for $\gamma > 2$; this agreement progressively worsens as γ is decreased from 2 to 0. The agreement can be made almost exact by adjusting β ; however, this will destroy self-similarity observed in Figures 9 and 10. The reasons behind this discrepancy will be explored in a future work.

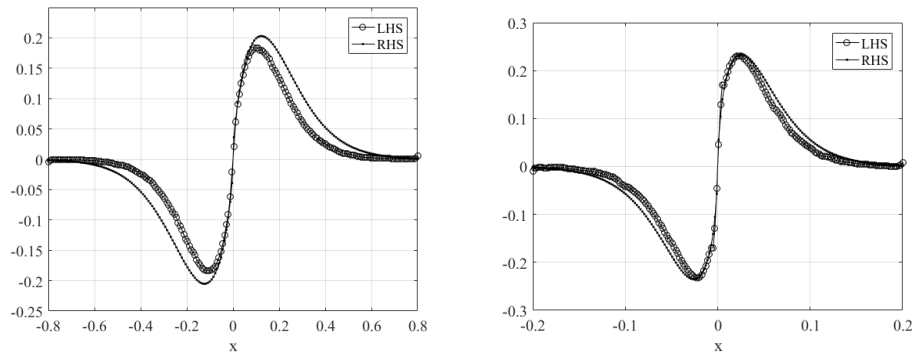


FIGURE 11. Comparing the right hand side and left hand side of (4.9).
Left: $\gamma = 2$. Right: $\gamma = 3$.

4.4. General relationship between steady-state distributions. Taking the Fourier transform of (4.4) with $\beta = \frac{\gamma}{2}$, we have

$$(4.10) \quad -\frac{\gamma}{2}k\hat{p}'_0(k) = -\hat{\mu}_0(k)\hat{p}_0(k) + \hat{p}_0(k),$$

where $\hat{p}_0(k) = \mathcal{F}(p_0(x))$ and $\hat{\mu}_0(k) = \mathcal{F}(\mu_0(x))$. Then (4.10) can be written as

$$(4.11) \quad \frac{1}{2} \frac{\hat{p}'_0(k)}{\hat{p}_0(k)} = \frac{\hat{\mu}_0(k) - 1}{\gamma k} \Rightarrow \hat{p}_0(k) = \exp\left(\frac{2}{\gamma} \int_0^k \frac{\hat{\mu}_0(k) - 1}{k} dk\right).$$

Condition (4.11) indicates that the initial distribution of velocities p_0 and the initial distribution of velocity jump sizes μ_0 depend on each other. Hence it is sufficient to check (4.11) to know if (4.1) and (4.2) satisfy (2.9). Furthermore, we can use (4.11) to solve for the non-trivial distribution μ_0 , i.e.,

$$(4.12) \quad \hat{\mu}_0(k) = \frac{\gamma k \hat{p}'_0(k)}{2 \hat{p}_0(k)} + 1.$$

5. SUMMARY

In this work we consider a simplified one-dimensional coarsening model inspired by earlier work on modeling grain growth in polycrystals. We generalize the theory of continuous time random walks to the case of time-dependent jumps and derive the corresponding master equation that is shown to admit self-similar solutions. Extensive numerical tests confirm that this framework successfully describes the behavior of the velocity statistics harvested from the one-dimensional simulation.

6. ACKNOWLEDGEMENT

The authors express their deep gratitude to David Kinderlehrer for introducing them to the mathematics of grain growth, his constant encouragement, numerous invaluable insights, and inspiration along the way.

7. APPENDIX. SUPERPOSITION OF NONHOMOGENEOUS POISSON PROCESSES

Here we develop a connection between the arrival rates for an ensemble of independent walkers compared to that for a single walker.

Definition 2. [39] The counting process $\{n_t, t \geq 0\}$ is said to be a nonhomogeneous Poisson process with rate function $\lambda(t)$, if

- (1) $n_0 = 0$.
- (2) $n_t, t \geq 0$ has independent increments.
- (3) $P(n_{t+h} - n_t \geq 2) = o(h)$.
- (4) $P(n_{t+h} - n_t = 1) = \lambda(t)h + o(h)$.

Theorem 3. Let $\{n_i(t)\}_{i=1}^R$ be independent nonhomogeneous Poisson processes with rate $\lambda(t)$. Define $n_t = \sum_{i=1}^R n_i(t)$. Then n_t is a nonhomogeneous Poisson process with rate $\lambda_R(t) = R\lambda(t)$.

Proof. We test conditions (1-4) in Definition 2. We start with condition (1),

$$n_0 = \sum_{i=1}^R n_i(0) = \sum_{i=1}^R 0 = 0.$$

Condition (2) follows from the independence assumption of $\{n_i(t)\}_{i=1}^R$. Condition (4) follows from,

$$\begin{aligned} P[n_{t+h} - n_t = 1] &= \sum_{i=1}^R P[n_i(t+h) - n_i(t) = 1] \prod_{j \neq i} P[n_j(t+h) - n_j(t) = 0] \\ &= \sum_{i=1}^R (\lambda(t)h + o(h)) \prod_{j \neq i} (1 - \lambda(t)h + o(h)) \\ &= \sum_{i=1}^R (\lambda(t)h + o(h)) (1 - \lambda(t)h + o(h))^{R-1} \\ &= R(\lambda(t)h + o(h)) (1 - \lambda(t)h + o(h))^{R-1} \\ &= R\lambda(t)h + o(h) \\ &= \lambda_R(t)h + o(h). \end{aligned}$$

Lastly, condition (3) follows from an argument similar to (4). Hence n_t is a nonhomogeneous Poisson process with rate $\lambda_R(t) = R\lambda(t)$. \square

REFERENCES

- [1] J. Carr and R. Pego. Self-similarity in a coarsening model in one dimension. *Proc. R. Soc. London Ser. A*, 436(1898):569–583, 1992.
- [2] W.W. Mullins. A one dimensional nearest neighbor model of coarsening. *Technical report, Carnegie Mellon University, Department of Mathematical Sciences*, page <http://repository.cmu.edu/math>, 1991.
- [3] W.W. Mullins. The statistical particle growth law in self-similar coarsening. *Acta Metall. Mater.*, 39(9):2081–2090, 1991.
- [4] E.A. Lazar and R. Permantle. Coarsening in one dimension: Invariant and asymptotic states. *arXiv preprint*, page arXiv 1505.07893 [math.PR], 2015.
- [5] E.A. Lazar. The evolution of cellular structures via curvature flow. *PhD thesis Princeton*, 2011.
- [6] K. Barmak, M. Emelianenko, D. Golovaty, D. Kinderlehrer, and S. Ta’asan. Towards a statistical theory of texture evolution in polycrystals. *SIAM J. of Sc. Comput.*, 30(6):3150–3169, 2008.
- [7] W.W. Mullins. The statistical self-similarity hypothesis in grain growth and particle coarsening. *J. Appl. Phys.*, 59:1341–1349, 1986.
- [8] W.W. Mullins and J. Vinals. Self-similarity and growth kinetics driven by surface free energy reduction. *Acta Metall. Mater.*, 37(4):991–997, 1989.
- [9] R.V. Kohn and F. Otto. Upper bounds on coarsening rates. *Commun. Math. Phys.*, 229:375–95, 2002.
- [10] R.V. Kohn and X. Yan. Upper bounds on the coarsening rate for an epitaxial growth model. *Commun. Pure Appl. Math.*, 56:1549–64, 2003.
- [11] R.V. Kohn and X. Yan. Coarsening rates for models of multicomponent phase separation. *Interfaces Free Bound*, 6:135–49, 2004.
- [12] S. Dai and R.L. Pego. Universal bounds on coarsening rates for mean field models of phase transitions. *SIAM J. Math. Anal.*, 37:347–71, 2005.
- [13] D. Slepcev. Coarsening in nonlocal interfacial systems. *SIAM J. Math. Anal.*, 40(3):1029–1048, 2008.
- [14] E.A. Lazar, J.K. Mason, R.D. MacPherson, and D.J. Srolovitz. A more accurate three-dimensional grain growth algorithm. *Acta Mater.*, 59(17):6837–6847, 2011.
- [15] J.K. Mason, E.A. Lazar, R.D. MacPherson, and D.J. Srolovitz. Statistical topology of cellular networks in two and three dimensions. *Phys. Rev. E*, 86(5):051128, 2012.

- [16] E. Scalas. The application of continuous-time random walks in finance and economics. *Physica A*, 362:225–239, 2006.
- [17] F. Mainardi, M. Raberto, R. Gorenflo, and E. Scalas. Fractional calculus and continuous time finance II: The waiting time distribution. *Physica A*, 287:468–481, 2000.
- [18] E. Scalas, R. Gorenflo, and F. Mainardi. Fractional calculus and continuous-time finance. *Physica A*, 284:376–384, 2000.
- [19] R. Gorenflo, F. Mainardi, E. Scalas, and M. Raberto. *Fractional calculus and continuous-time finance III: The diffusion limit*. In: *Trends in Mathematics - Mathematical Finance*. Birkhauser, 2001.
- [20] H.G. Othmer, S.R. Dunbar, and W. Alt. Models of dispersal in biological systems. *J. Math. Biol.*, 26:263–298, 1988.
- [21] H.G. Othmer and C. Xue. *The mathematical analysis of biological aggregation and dispersal: progress, problems, and perspectives*. In: *Dispersal, Individual Movement and Spatial Ecology: A Mathematical Perspective*. Springer, Heidelberg, 2013.
- [22] B.Ph. van Milligen, R. Sanchez, and B.A. Carreras. Probabilistic finite-size transport models for fusion: Anomalous transport and scaling laws. *Phys. Plasmas*, 11(5):2272–2285, 2004.
- [23] C.N. Angstmann, I.C. Donnelly, and B.I. Henry. Continuous time random walks with reactions forcing and trapping. *Math. Model. Nat. Phenom.*, 8(2):17–27, 2013.
- [24] C.N. Angstmann, I.C. Donnelly, and B.I. Henry. Pattern formation on networks with reactions: A continuous-time random-walk approach. *Phys. Rev. E*, 87:032804, 2013.
- [25] C.N. Angstmann, I.C. Donnelly, B.I. Henry, T.A.M. Langlands, and P. Straka. Continuous-time random walks on networks with vertex and time-dependent forcing. *Phys. Rev. E*, 88:022811, 2013.
- [26] J. Klafter, A. Blumen, and M.F. Shlesinger. Stochastic pathway to anomalous diffusion. *Phys. Rev. A*, 35(7):3081–3085, 1987.
- [27] R. Metzler and J. Klafter. The random walk’s guide to anomalous diffusion: A fractional dynamics approach. *Phys. Rep.*, 339:1–77, 2000.
- [28] R. Hilfer and L. Anton. Fractional master equations and fractal time random walks. *Phys. Rev. E*, 51:R848, 1995.
- [29] E. Barkai, R. Metzler, and J. Klafter. From continuous time random walks to the fractional Fokker-Planck equation. *Phys. Rev. E*, 61(1):132–138, 2000.
- [30] F. Mainardi, R. Gorenflo, and E. Scalas. A fractional generalization of the Poisson processes. *Vietnam J. of Math.*, 32:53–64, 2007.
- [31] E. Scalas, R. Gorenflo, F. Mainardi, and M. Raberto. Revisiting the derivation of the fractional diffusion equation. *Fractals*, 11:281–289, 2003.
- [32] C.N. Angstmann, I.C. Donnelly, B.I. Henry, T.A.M. Langlands, and P. Straka. Generalized continuous time random walks, master equations, and fractional fokker-planck equations. *SIAM J. of Appl. Math.*, 75(4):1445–1468, 2015.
- [33] E. Scalas, R. Gorenflo, and F. Mainardi. Uncoupled continuous-time random walks: Solution and limiting behavior of the master equation. *Phys. Rev. E*, 69:011107, 2004.
- [34] K. Barmak, M. Emelianenko, D. Golovaty, D. Kinderlehrer, and S. Ta’asan. A new perspective on texture evolution. *Int. J. Numer. Anal. and Model.*, 5:3–108, 2008z.
- [35] K. Barmak, E. Eggeling, M. Emelianenko, Y. Epshteyn, D. Kinderlehrer, R. Sharp, and S. Ta’asan. Critical events, entropy, and the grain boundary character distribution. *Phys. Rev. B*, 83:134117, 2011.
- [36] E.W. Montroll and G.H. Weiss. Random walks on lattices II. *J. Math. Phys.*, 6(2):167–181, 1965.
- [37] W.W. Montroll and H. Scher. Random walks on lattices, IV: Continuous-time walks and influence of absorbing boundaries. *J. Stat. Phys.*, 9:101–135, 1973.
- [38] J. Klafter and R. Silbey. Derivation of the continuous time random walk equation. *Phys. Rev. Lett.*, 44(2):55–58, 1980.
- [39] S.M. Ross. *Introduction to Probability Models*. Academic Press, New York, 2010.

DEPARTMENT OF MATHEMATICAL SCIENCES, GEORGE MASON UNIVERSITY, FAIRFAX, VA 22030
 E-mail address: dtorrejo@masonlive.gmu.edu, memelian@gmu.edu

DEPARTMENT OF MATHEMATICS, THE UNIVERSITY OF AKRON, AKRON, OH 44325
 E-mail address: dmitry@uakron.edu